

Shape Optimization with Nonlinear Conjugate Gradient Methods

Sebastian Blauth

This is a post-peer-review, pre-copyedit version of an article published in Lecture Notes in Computational Science and Engineering, Volume 137. The final version is available online at https://doi.org/10.1007/978-3-031-20432-6_9.

Abstract In this chapter, we investigate recently proposed nonlinear conjugate gradient (NCG) methods for shape optimization problems. We briefly introduce the methods as well as the corresponding theoretical background and investigate their performance numerically. The obtained results confirm that the NCG methods are efficient and attractive solution algorithms for shape optimization problems.

1 Introduction

Shape optimization problems arise in many industrial applications, such as the design optimization of airplanes [27], automobiles [23], electric motors [11], microchannel systems [5,6], polymer spin packs [16,20], and melting furnaces [19]. For the solution of such problems, shape optimization based on shape calculus (see, e.g., [8]) has attracted lots of research interest in recent years, with particular regards to the development of efficient solution algorithms. This can be seen, e.g., in [28] and [29], where Newton and limited memory BFGS (L-BFGS) methods for shape optimization are proposed, respectively, and in [9,22], where special mesh deformation procedures for increasing the mesh quality and the avoidance of remeshing are investigated.

In this chapter, we consider the recently proposed nonlinear conjugate gradient (NCG) methods for shape optimization from [4], which are numerical solution algorithms for such problems, and investigate their performance. One of the benefits of these NCG methods is that they require only slightly more memory than the popular gradient descent method, while being significantly more efficient. Here, we

Sebastian Blauth
Fraunhofer ITWM, Fraunhofer-Platz 1, 67663 Kaiserslautern e-mail: sebastian.blauth@itwm.fraunhofer.de

compare the numerical performance of the NCG methods to the already established gradient descent and L-BFGS methods for shape optimization. For this numerical comparison we utilize our software package cashocs [3] which implements these methods and allows for a detailed comparison.

This chapter is structured as follows. In Sect. 2, we briefly present some theoretical background on shape optimization and shape calculus. This is required for the presentation of the nonlinear conjugate gradient methods in Sect. 3. Finally, the numerical examples, which showcase the capabilities of the NCG methods, can be found in Sect. 4.

2 Theoretical Background

In this section, we present some theoretical background on shape optimization and shape calculus which we require for our presentation of the NCG methods in Sect. 3.

2.1 Fundamentals of Shape Optimization

A general shape optimization problem with a partial differential equation (PDE) as constraint is given by

$$\begin{aligned} & \min_{\Omega, u} \mathcal{J}(\Omega, u) \\ & \text{subject to} \quad e(\Omega, u) = 0, \\ & \quad \quad \quad \Omega \in \mathcal{A}. \end{aligned} \tag{1}$$

Here, \mathcal{J} is a cost functional which we want to minimize over a set of admissible geometries $\mathcal{A} \subset \{ \Omega \subset D \}$ for some given bounded hold-all domain $D \subset \mathcal{R}^d$ and u is the so-called state variable which lies in the state space $U(\Omega)$. Additionally, $e(\Omega, \cdot): U(\Omega) \rightarrow V(\Omega)^*$, where $V(\Omega)^*$ is the dual space of $V(\Omega)$, is an operator that models the PDE constraint, which we interpret in the weak form

$$\text{Find } u \in U(\Omega) \text{ such that } \langle e(\Omega, u), v \rangle_{V(\Omega)^*, V(\Omega)} = 0 \quad \text{for all } v \in V(\Omega). \tag{2}$$

We assume that the state equation (2) admits a unique solution $u = u(\Omega)$ for all $\Omega \in \mathcal{A}$ so that we have $e(\Omega, u(\Omega)) = 0$. With this, we can introduce the reduced cost functional $J(\Omega) = \mathcal{J}(\Omega, u(\Omega))$ and rephrase (1) equivalently as

$$\min_{\Omega} J(\Omega) \quad \text{subject to} \quad \Omega \in \mathcal{A}, \tag{3}$$

where we have formally eliminated the PDE constraint.

2.2 Shape Calculus

To obtain efficient solution algorithms for problem (1), one can use techniques from shape calculus to derive sensitivities of the cost functional $J(\Omega)$ w.r.t. variations of the domain Ω . In the following, we briefly recall these techniques and we refer to, e.g., [8] for an exhaustive treatment of this topic.

We define a family of deformed domains Ω_t for $t \geq 0$ as

$$\Omega_t = F_t(\Omega) = \{ F_t(x) \mid x \in \Omega \}.$$

In this chapter, we use the so-called perturbation of identity (cf. [8]), in which the transformation F_t is given by

$$F_t(x) = (I + t\mathcal{V})(x),$$

where I denotes the identity matrix in \mathbb{R}^d and \mathcal{V} is a vector field in $C_0^k(D; \mathbb{R}^d)$ for some $k \geq 1$, i.e., the space of k -times continuously differentiable functions from D to \mathbb{R}^d with compact support. Note, that there exist other, equivalent approaches for calculating first order shape derivatives, such as the speed method (cf. [8]), but for the sake of brevity we only consider the perturbation of identity in this chapter. Now, we can define the shape derivative as follows (cf. [8, Chapter 9, Definition 3.4]).

Definition 1 Let $\tau > 0$ be sufficiently small, $\mathcal{A} \subset \{ \Omega \subset D \}$, $J: \mathcal{A} \rightarrow \mathbb{R}$, and $\Omega \in \mathcal{A}$. Additionally, let $\mathcal{V} \in C_0^k(D; \mathbb{R}^d)$ with $k \geq 1$, let $F_t = I + t\mathcal{V}$ be the perturbation of identity with \mathcal{V} , and assume that $\Omega_t = F_t(\Omega) \in \mathcal{A}$ for all $t \in [0, \tau]$.

We say that J has a Eulerian semi-derivative at Ω in direction \mathcal{V} if the limit

$$dJ(\Omega)[\mathcal{V}] := \lim_{t \searrow 0} \frac{J(F_t(\Omega)) - J(\Omega)}{t} = \left. \frac{d}{dt} J(F_t(\Omega)) \right|_{t=0^+}$$

exists. Moreover, let Ξ be a topological vector subspace of $C_0^\infty(D; \mathbb{R}^d)$. We say that J is shape differentiable at Ω w.r.t. Ξ if it has a Eulerian semi-derivative at Ω in all directions $\mathcal{V} \in \Xi$ and, additionally, the mapping

$$dJ(\Omega): \Xi \rightarrow \mathbb{R}; \quad \mathcal{V} \mapsto dJ(\Omega)[\mathcal{V}]$$

is linear and continuous. In this case, we call $dJ(\Omega)[\mathcal{V}]$ the shape derivative of J at Ω w.r.t. Ξ in direction $\mathcal{V} \in \Xi$.

Note, that there exist several possibilities for calculating shape derivatives in the context of PDE constrained shape optimization, an overview of which can, e.g., be found in [30]. These methods involve solving a so-called adjoint equation to calculate the shape derivative, which is usual in PDE constrained optimization (cf. [15]).

An important result from shape calculus is Hadamard's structure theorem, which we briefly recall here.

Theorem 1 (Structure Theorem) *Let J be a shape functional which is shape differentiable at some $\Omega \subset D$ and let $\Gamma = \partial\Omega$ be compact. Further, let $k \geq 0$ be the*

smallest integer such that $dJ(\Omega) : C_0^\infty(D; \mathbb{R}^d) \rightarrow \mathbb{R}$; $\mathcal{V} \mapsto dJ(\Omega)[\mathcal{V}]$ is continuous w.r.t. the $C_0^k(D; \mathbb{R}^d)$ topology, and assume that Γ is of class C^{k+1} . Then, there exists a continuous, linear functional $g : C^k(\Gamma) \rightarrow \mathbb{R}$ such that

$$dJ(\Omega)[\mathcal{V}] = g[\mathcal{V} \cdot n],$$

where n is the outer unit normal vector on Γ . In particular, if $g \in L^1(\Gamma)$, it holds that

$$dJ(\Omega)[\mathcal{V}] = \int_{\Gamma} g \mathcal{V} \cdot n \, ds.$$

Proof The proof can be found in [8, Theorem 3.6 and Corollary 1, pp. 479–481]. \square

2.3 A Riemannian View on Shape Optimization and Steklov-Poincaré-Type Metrics

In order to formulate the nonlinear CG methods for shape optimization, we now briefly recall the Riemannian view on shape optimization from [28] as well as the corresponding Steklov-Poincaré-type metrics from [29].

We consider compact and connected subsets $\Omega \subset D \subset \mathbb{R}^2$ with C^∞ boundary, where D is, again, some bounded hold-all domain. As in [28], we define

$$B_e(S^1; \mathbb{R}^2) := \text{Emb}(S^1; \mathbb{R}^2) / \text{Diff}(S^1),$$

i.e., the set of all equivalence classes of C^∞ embeddings of the unit circle $S^1 \subset \mathbb{R}^2$ into \mathbb{R}^2 , given by $\text{Emb}(S^1; \mathbb{R}^2)$, where the equivalence relation is defined via the set of all C^∞ diffeomorphisms of S^1 into itself, given by $\text{Diff}(S^1)$. Note, that this equivalence relation factors out reparametrizations as these do not change the underlying shape. It is shown in [18] that B_e , which is the set of all smooth two-dimensional shapes, is a smooth manifold. An element of $B_e(S^1; \mathbb{R}^2)$ is represented by a smooth curve $\Gamma : S^1 \rightarrow \mathbb{R}^2$; $\theta \mapsto \Gamma(\theta)$. Due to the equivalence relation, the tangent space at $\Gamma \in B_e$ is isomorphic to the set of all C^∞ normal vector fields along Γ , i.e.,

$$T_\Gamma B_e \cong \{ h \mid h = \alpha n, \alpha \in C^\infty(\Gamma; \mathbb{R}) \} \cong \{ \alpha \mid \alpha \in C^\infty(\Gamma; \mathbb{R}) \}.$$

As in [29], we consider the following Steklov-Poincaré-type metric g_Γ^S at some $\Gamma \in B_e$, which is defined as

$$g_\Gamma^S : H^{1/2}(\Gamma) \times H^{1/2}(\Gamma) \rightarrow \mathbb{R}; (\alpha, \beta) \mapsto \int_{\Gamma} \alpha (S_\Gamma^P)^{-1} \beta \, ds. \quad (4)$$

Here, S_Γ^P is a symmetric and coercive operator defined by

$$S_\Gamma^P : H^{-1/2}(\Gamma) \rightarrow H^{1/2}(\Gamma); \alpha \mapsto U \cdot n,$$

where $U \in H^1(\Omega)^d$ solves the problem

$$\text{Find } U \in H^1(\Omega)^d \text{ such that } a_\Omega(U, V) = \int_\Gamma \alpha (V \cdot n) \, ds \quad \text{for all } V \in H^1(\Omega)^d, \quad (5)$$

for a symmetric, continuous, and coercive bilinear form $a_\Omega: H^1(\Omega)^d \times H^1(\Omega)^d \rightarrow \mathbb{R}$. To define a Riemannian metric on B_e , we restrict g^S to the tangent space $T_\Gamma B_e$.

Let us now briefly discuss the relation between the metric g_Γ^S and shape calculus. To do so, we assume that the shape functional J is shape differentiable and has a shape derivative of the form

$$dJ(\Omega)[\mathcal{V}] = \int_\Gamma g \, \mathcal{V} \cdot n \, ds,$$

with $g \in L^2(\Gamma)$ (cf. Theorem 1). Then, the Riemannian shape gradient w.r.t. g_Γ^S is given by $\gamma \in T_\Gamma B_e$, which is the solution of

$$\text{Find } \gamma \in T_\Gamma B_e \text{ such that } g_\Gamma^S(\gamma, \phi) = \int_\Gamma g \phi \, ds \quad \text{for all } \phi \in T_\Gamma B_e. \quad (6)$$

Due to the definition of g_Γ^S , the solution of (6) is given by $\gamma = S_\Gamma^p g$, in particular, we have that $\gamma = \mathcal{G} \cdot n$, where \mathcal{G} solves

$$\text{Find } \mathcal{G} \in H^1(\Omega)^d \text{ such that } a_\Omega(\mathcal{G}, \mathcal{V}) = dJ(\Omega)[\mathcal{V}] \quad \text{for all } \mathcal{V} \in H^1(\Omega)^d. \quad (7)$$

Due to the Lax-Milgram lemma, this problem has a unique solution \mathcal{G} which we call the gradient deformation of J at Ω . The gradient deformation \mathcal{G} can be interpreted as an extension of the shape gradient γ to the entire domain Ω . Since a_Ω is coercive, there exists a constant $C > 0$ so that

$$dJ(\Omega)[- \mathcal{G}] = a_\Omega(- \mathcal{G}, \mathcal{G}) \leq -C \|\mathcal{G}\|_{H^1(\Omega)}^2 \leq 0, \quad (8)$$

i.e., an infinitesimal perturbation of identity with the negative gradient deformation yields a descent in the shape functional J . This fact is often used for the solution of shape optimization problems with a gradient descent method (see, e.g., [9, 16]).

3 Nonlinear CG Methods for Shape Optimization

We now use the theoretical framework introduced in Sect. 2 to formulate our NCG methods for shape optimization from [4]. To do so, we consider only reduced shape optimization problems of the form (3). For the sake of brevity, we only focus on a theoretical description of the methods. However, a detailed description of our numerical implementation of the methods can be found in our previous work [4].

Starting from an initial guess Ω_0 , the k -th iteration of the NCG methods consists of the following steps: First, we compute the shape derivative $dJ(\Omega)[\cdot]$ of our cost

Algorithm 1: Nonlinear CG methods for shape optimization.

Input: Initial geometry Ω_0 , represented by its boundary Γ_0
for $k=0, 1, 2, \dots, k_{max}$ **do**
 Compute the shape derivative $dJ(\Omega_k)[\cdot]$
 Compute the Riemannian shape gradient γ_k by solving (6)
 if *Stopping criterion is satisfied* **then**
 Stop with approximate solution Γ_k
 Compute the search direction $\delta_k = -\gamma_k + \beta_k \mathcal{T}_{\eta_{k-1}} \delta_{k-1}$
 Compute a feasible step size t_k
 Set $\eta_k = t_k \delta_k$ and update the geometry $\Gamma_{k+1} = R_{\Gamma_k} \eta_k$

functional J which involves solving the state and adjoint equation on the domain Ω_k (cf. [4]). Next, we compute the Riemannian shape gradient γ_k via equation (6). Note, that this involves the computation of the gradient deformation (cf. equation (7)), which is beneficial for our numerical implementation of the method as described detailedly in [4]. The next step of the methods involves the computation of the search direction δ_k , which is defined as

$$\delta_k = -\gamma_k + \beta_k \mathcal{T}_{\eta_{k-1}} \delta_{k-1},$$

where we set $\delta_0 = -\gamma_0$. Here, the parameter η_{k-1} is defined as $\eta_{k-1} = t_{k-1} \delta_{k-1}$ with the previous step size t_{k-1} (see below) and \mathcal{T} denotes a vector transport (see, e.g., [1, 26] for more details). Moreover, the parameter β_k is an update parameter for the NCG method, which is detailed below. After we have obtained the search direction, we have to compute a feasible step size for updating our domain. This can be accomplished with, e.g., an Armijo line search (cf. [4] for more details) and yields the step size t_k for iteration k . The geometry is then updated with the help of an retraction R (see, e.g., [1, 26] for more details), i.e.,

$$\Gamma_{k+1} = R_{\Gamma_k} \eta_k,$$

where η_k is the scaled search direction for iteration k , i.e., $\eta_k = t_k \delta_k$. Finally, we increment k and proceed as before, until an appropriate stopping criterion is reached (cf. [4]). Note, that an algorithmic description of this procedure is given in Algorithm 1.

We consider five different NCG variants, namely the NCG methods of Fletcher and Reeves (FR) [10], Polak and Ribiere (PR) [25], Hestenes and Stiefel (HS) [14], Dai and Yuan (DY) [7], and Hager and Zhang (HZ) [12]. Note, that an overview over these methods for finite-dimensional problems can be found, e.g., in [13]. The update parameters β in the context of shape optimization are given by

$$\beta_k^{\text{FR}} = \frac{g_{\Gamma_k}^S(\gamma_k, \gamma_k)}{g_{\Gamma_k}^S(\mathcal{T}_{\eta_{k-1}} \gamma_{k-1}, \mathcal{T}_{\eta_{k-1}} \gamma_{k-1})},$$

$$\begin{aligned}
\beta_k^{\text{PR}} &= \frac{g_{\Gamma_k}^S(\gamma_k, y_{k-1})}{g_{\Gamma_k}^S(\mathcal{T}_{\eta_{k-1}}\gamma_{k-1}, \mathcal{T}_{\eta_{k-1}}\gamma_{k-1})}, \\
\beta_k^{\text{HS}} &= \frac{g_{\Gamma_k}^S(\gamma_k, y_{k-1})}{g_{\Gamma_k}^S(\mathcal{T}_{\eta_{k-1}}d_{k-1}, y_{k-1})}, \\
\beta_k^{\text{DY}} &= \frac{g_{\Gamma_k}^S(\gamma_k, \gamma_k)}{g_{\Gamma_k}^S(\mathcal{T}_{\eta_{k-1}}d_{k-1}, y_{k-1})}, \\
\beta_k^{\text{HZ}} &= g_{\Gamma_k}^S \left(y_{k-1} - 2\mathcal{T}_{\eta_{k-1}}d_{k-1} \frac{g_{\Gamma_k}^S(y_{k-1}, y_{k-1})}{g_{\Gamma_k}^S(\mathcal{T}_{\eta_{k-1}}d_{k-1}, y_{k-1})}, \frac{\gamma_k}{g_{\Gamma_k}^S(\mathcal{T}_{\eta_{k-1}}d_{k-1}, y_{k-1})} \right),
\end{aligned}$$

where we use

$$y_{k-1} = \gamma_k - \mathcal{T}_{\eta_{k-1}}\gamma_{k-1}.$$

A particular advantage of the NCG methods is the following: The NCG methods only require one or two additional vectors of storage compared to the popular gradient descent method, while being substantially more efficient, as is shown in Sect. 4. The L-BFGS methods with memory size m , on the other hand, require $2m$ additional vectors of storage, which can be prohibitive for very large scale problems, such as the ones arising from industrial applications (see [17]). Hence, the NCG methods are particularly interesting for these kinds of problems, where memory requirements are of great importance.

4 Numerical Examples

In this section, we investigate the previously introduced NCG methods numerically on two benchmark problems. In Sect. 4.1, we consider a two-dimensional shape optimization problem with a Poisson equation as PDE constraint and in Sect. 4.2, we consider the drag minimization in a three-dimensional pipe. For both test cases, we compare the five NCG variants from Sect. 3 to the gradient descent and L-BFGS methods. The numerical implementation is done in our software cashocs [3], which is based on the finite element software FEniCS [2, 21], and we refer to our previous work [4] for a comprehensive description of our implementation of the NCG methods.

4.1 Shape Optimization with a Poisson Equation

The first test case is taken from [4, 9] and is given by

$$\begin{aligned}
\min_{\Omega} J(\Omega, u) &= \int_{\Omega} u \, dx \\
\text{subject to} \quad & -\Delta u = f \quad \text{in } \Omega, \\
& u = 0 \quad \text{on } \Gamma,
\end{aligned} \tag{9}$$

where we consider the problem in two dimensions and use

$$f(x) = 2.5 \left(x_1 + 0.4 - x_2^2 \right)^2 + x_1^2 + x_2^2 - 1.$$

Our initial guess Ω_0 is given by the unit disc in \mathbb{R}^2 . We discretize the PDE constraint with piecewise linear Lagrange elements, for which we use a uniform mesh consisting of 7651 nodes and 15 000 triangles.

We solve this problem with the gradient descent (GD) method, a L-BFGS method with memory size $m = 5$ (L-BFGS 5), and the five NCG methods presented in Sect. 3. The history of the optimization can be seen in Fig. 1, where the evolution of the cost functional (Fig. 1a) and relative gradient norm (Fig. 1b) are shown. Here, we have highlighted the graphs of the gradient descent, L-BFGS 5, and the NCG variant of Dai and Yuan (NCG DY), as the latter performed best of all NCG methods. For the sake of better readability, the remaining NCG methods are shown in transparent colors. Here, we observe that all NCG methods perform significantly better than the gradient descent method, as they reach the optimal function value faster and also have lower gradient norms throughout the optimization. On average, the NCG methods achieve a gradient norm that is one order of magnitude smaller than the gradient norm obtained with the gradient descent method. However, the performance of the L-BFGS 5 method is still slightly better than that of the NCG methods, but this comes at the cost of a higher memory usage, as discussed previously.

A visual inspection of the optimized geometries, which can be found in Fig. 2, shows that the NCG methods perform very well. Here, the optimized geometries for the gradient descent, Fletcher-Reeves NCG and Polak-Ribiere NCG methods are shown and compared to the reference solution (computed with the L-BFGS 5 method). We observe, that there are still visible differences between the reference solution and the one obtained with the gradient descent method, particularly in the

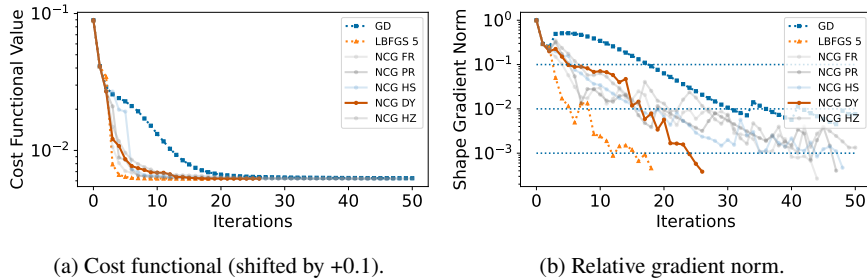


Fig. 1: History of the optimization methods for problem (9).

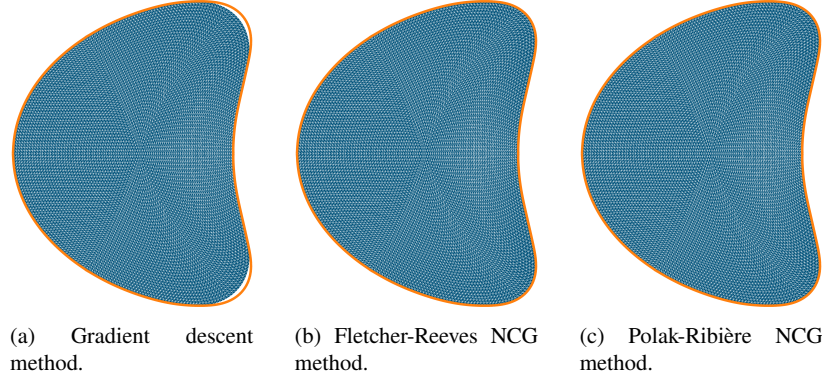


Fig. 2: Optimized Shapes (blue) compared to the reference solution (orange) for the Poisson problem (9).

right corners of the geometry. The two NCG methods, however, show no visible differences compared to the reference domain, which underlines their improved convergence behavior compared to the gradient descent method.

4.2 Shape Optimization of Energy Dissipation in a Pipe

For our second test case, we consider the problem of reducing the energy dissipation of a fluid in a three-dimensional pipe, which is taken from [24]. Here, the flow of the fluid is governed by the Navier-Stokes equations. The corresponding shape optimization problem is given by

$$\begin{aligned}
 \min_{\Omega} J(\Omega, u) &= \frac{1}{\text{Re}} \int_{\Omega} \varepsilon(u) : \varepsilon(u) \, dx + \frac{\gamma}{2} \left(\int_{\Omega} 1 \, dx - \int_{\Omega_0} 1 \, dx \right)^2 \\
 \text{subject to} \quad & -\frac{2}{\text{Re}} \nabla \cdot \varepsilon(u) + (u \cdot \nabla) u + \nabla p = 0 \quad \text{in } \Omega, \\
 & \nabla \cdot u = 0 \quad \text{in } \Omega, \\
 & u = u^{\text{in}} \quad \text{on } \Gamma^{\text{in}}, \\
 & u = 0 \quad \text{on } \Gamma^{\text{wall}}, \\
 & \frac{2}{\text{Re}} \varepsilon(u)n - pn = 0 \quad \text{on } \Gamma^{\text{out}}.
 \end{aligned} \tag{10}$$

Here, u denotes the flow velocity, p the pressure and $\varepsilon(u) = 1/2(\nabla u + \nabla u^T)$ is the symmetric gradient of u . Note, that the cost functional consists of two terms, where the first one measures the energy dissipation in the pipe and the second one is a regularization of a volume equality constraint. The latter is used to constrain the vol-

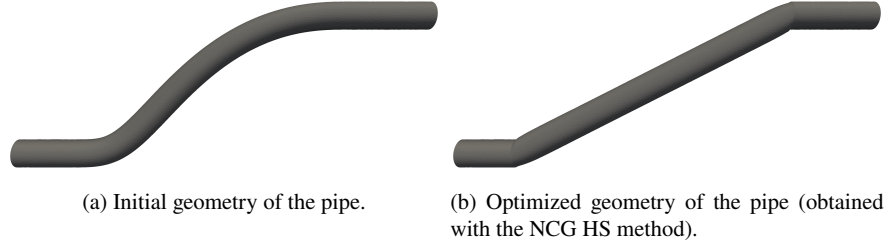


Fig. 3: Initial and optimized geometries for problem (10).

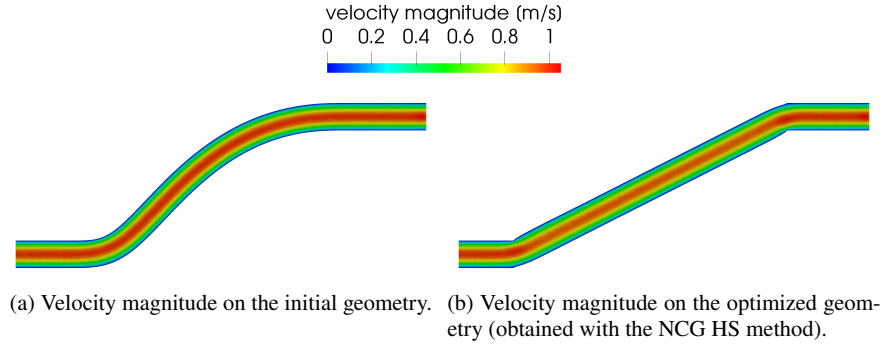


Fig. 4: Velocity magnitude on the initial and optimized geometries, shown as slice through the middle of the geometry.

ume of the pipe to its initial volume. Moreover, the pipe's boundary Γ is partitioned into the inlet Γ^{in} and the wall boundary Γ^{wall} , where we use Dirichlet boundary conditions, as well as the outlet Γ^{out} , where we use a do-nothing boundary condition. We discretize the geometry with 17 873 nodes and 82 422 tetrahedrons. Additionally, we discretize the Navier-Stokes equations with the inf-sup-stable Taylor-Hood elements, i.e., piecewise quadratic Lagrange elements for the velocity and piecewise linear Lagrange elements for the pressure. Note, that a plot of the initial and optimized geometries is shown in Fig. 3, and that the velocity magnitude on these domains is visualized in Fig. 4.

As before, we solve this shape optimization problem with the gradient descent, L-BFGS 5, and the NCG methods, where we consider the case of laminar flow and use a Reynolds number of $\text{Re} = 1$ as well as a penalty parameter of $\gamma = 100$. Note, that the choice of γ is sufficiently large to ensure a relative volume difference below 0.5 % between the initial and optimized geometries for all methods, so that the equality constraint is satisfied numerically. The corresponding results of the optimization are shown in Fig. 5, where, again, the history of the cost functional (cf. Fig. 5a) and the relative gradient norm (cf. Fig. 5b) are shown. Here, we again observe that the NCG methods are very efficient. The best performing NCG method is, again, the

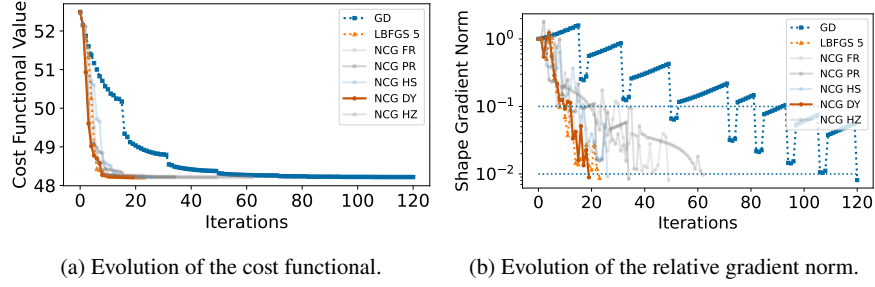


Fig. 5: History of the optimization methods for problem (10).

one of Dai and Yuan (DY), which even slightly outperformed the L-BFGS 5 method. Additionally, the method of Hestenes and Stiefel (HS) also performed very well and was only slightly worse than the L-BFGS method. The remaining NCG variants performed a bit worse, but all of them were substantially better than the gradient descent method as they required less than half the amount of iterations to reach the prescribed relative tolerance for this problem.

5 Conclusions

In this chapter, we have presented and investigated the nonlinear conjugate gradient (NCG) methods for shape optimization from [4]. After recalling recent results from shape optimization and shape calculus, we formulated the NCG methods in the Riemannian setting for shape optimization introduced in [28, 29]. Afterwards, we investigated these methods numerically and compared them to the already established gradient descent and L-BFGS methods for shape optimization. The results show that the NCG methods perform substantially better than the popular gradient descent method and that their performance is comparable to the one of the L-BFGS methods from [29]. Hence, the NCG methods could be particularly interesting for large-scale industrial problems due to their efficiency and low memory requirements.

References

1. Absil, P.A., Mahony, R., Sepulchre, R.: Optimization algorithms on matrix manifolds. Princeton University Press, Princeton, NJ (2008)
2. Alnæs, M.S., Blechta, J., Hake, J., Johansson, A., Kehlet, B., Logg, A., Richardson, C., Ring, J., Rognes, M.E., Wells, G.N.: The FEniCS project version 1.5. *Archive of Numerical Software* **3**(100) (2015)
3. Blauth, S.: cashocs: A Computational, Adjoint-Based Shape Optimization and Optimal Control Software. *SoftwareX* **13**, 100646 (2021)

4. Blauth, S.: Nonlinear Conjugate Gradient Methods for PDE Constrained Shape Optimization Based on Steklov-Poincaré-Type Metrics. *SIAM J. Optim.* **31**(2), 1658–1689 (2021)
5. Blauth, S., Leithäuser, C., Pinnau, R.: Model hierarchy for the shape optimization of a microchannel cooling system. *ZAMM Z. Angew. Math. Mech.* p. e202000166 (2020)
6. Blauth, S., Leithäuser, C., Pinnau, R.: Shape sensitivity analysis for a microchannel cooling system. *J. Math. Anal. Appl.* **492**(2), 124476 (2020)
7. Dai, Y.H., Yuan, Y.: A nonlinear conjugate gradient method with a strong global convergence property. *SIAM J. Optim.* **10**(1), 177–182 (1999)
8. Delfour, M.C., Zolésio, J.P.: Shapes and geometries, *Advances in Design and Control*, vol. 22, second edn. Society for Industrial and Applied Mathematics (SIAM), Philadelphia, PA (2011)
9. Etling, T., Herzog, R., Loayza, E., Wachsmuth, G.: First and second order shape optimization based on restricted mesh deformations. *SIAM J. Sci. Comput.* **42**(2), A1200–A1225 (2020)
10. Fletcher, R., Reeves, C.M.: Function minimization by conjugate gradients. *Comput. J.* **7**, 149–154 (1964)
11. Gangl, P., Langer, U., Laurain, A., Meftahi, H., Sturm, K.: Shape optimization of an electric motor subject to nonlinear magnetostatics. *SIAM J. Sci. Comput.* **37**(6), B1002–B1025 (2015)
12. Hager, W.W., Zhang, H.: A new conjugate gradient method with guaranteed descent and an efficient line search. *SIAM J. Optim.* **16**(1), 170–192 (2005)
13. Hager, W.W., Zhang, H.: A survey of nonlinear conjugate gradient methods. *Pac. J. Optim.* **2**(1), 35–58 (2006)
14. Hestenes, M.R., Stiefel, E.: Methods of conjugate gradients for solving linear systems. *J. Research Nat. Bur. Standards* **49**, 409–436 (1953) (1952)
15. Hinze, M., Pinnau, R., Ulbrich, M., Ulbrich, S.: Optimization with PDE constraints, *Mathematical Modelling: Theory and Applications*, vol. 23. Springer, New York (2009)
16. Hohmann, R., Leithäuser, C.: Shape optimization of a polymer distributor using an Eulerian residence time model. *SIAM J. Sci. Comput.* **41**(4), B625–B648 (2019)
17. Kelley, C.T.: Iterative methods for optimization, *Frontiers in Applied Mathematics*, vol. 18. Society for Industrial and Applied Mathematics (SIAM), Philadelphia, PA (1999)
18. Kriegl, A., Michor, P.W.: The convenient setting of global analysis, *Mathematical Surveys and Monographs*, vol. 53. American Mathematical Society, Providence, RI (1997)
19. Leithäuser, C., Pinnau, R.: Energy-Efficient High Temperature Processes via Shape Optimization, pp. 123–143. Springer International Publishing, Cham (2021)
20. Leithäuser, C., Pinnau, R., Feßler, R.: Designing polymer spin packs by tailored shape optimization techniques. *Optim. Eng.* **19**(3), 733–764 (2018)
21. Logg, A., Mardal, K.A., Wells, G.N., et al.: Automated Solution of Differential Equations by the Finite Element Method. Springer (2012)
22. Müller, P.M., Kühl, N., Siebenborn, M., Deckelnick, K., Hinze, M., Rung, P.: A novel p -harmonic descent approach applied to fluid dynamic shape optimization. *Structural and Multidisciplinary Optimization* **64**, 3489–3503 (2021)
23. Othmer, C.: Adjoint methods for car aerodynamics. *J. Math. Ind.* **4**, Art. 6, 23 (2014)
24. Paganini, A., Wechsung, F.: Fireshape: a shape optimization toolbox for Firedrake. *Struct. Multidiscip. Optim.* **63** (2021)
25. Polak, E., Ribière, G.: Note sur la convergence de méthodes de directions conjuguées. *Rev. Française Informat. Recherche Opérationnelle* **3**(16), 35–43 (1969)
26. Ring, W., Wirth, B.: Optimization methods on Riemannian manifolds and their application to shape space. *SIAM J. Optim.* **22**(2), 596–627 (2012)
27. Schmidt, S., Ilic, C., Schulz, V., Gauger, N.R.: Three-dimensional large-scale aerodynamic shape optimization based on shape calculus. *AIAA Journal* **51**(11), 2615–2627 (2013)
28. Schulz, V.H.: A Riemannian view on shape optimization. *Found. Comput. Math.* **14**(3), 483–501 (2014)
29. Schulz, V.H., Siebenborn, M., Welker, K.: Efficient PDE constrained shape optimization based on Steklov-Poincaré-type metrics. *SIAM J. Optim.* **26**(4), 2800–2819 (2016)
30. Sturm, K.: Shape differentiability under non-linear PDE constraints. In: New trends in shape optimization, *Internat. Ser. Numer. Math.*, vol. 166, pp. 271–300. Birkhäuser/Springer, Cham (2015)